which is the buckling equation for a long cylinder. Figure 6 shows the nonlinear stress patterns for one external pressure and two internal pressure conditions for a 1.4:1 elliptical head-to-cylinder juncture. External pressure causes a more significant change in the maximum stress than will a corresponding internal pressure. Thus to check experimentally a particular theoretical juncture region, externally pressurizing the actual configuration or a smaller model may prove more feasible than the actual internal pressurization method.

The nonlinear pressure vessel theory enables a structure analyst to design lighter missile cases. In low-pressure space stations of the future the parameter pR^2/Et^2 may become high enough so that the nonlinear theory must be used.

References

[1] Hetenyi, M., *Beams on Elastic Foundation* (The University of Michigan Press, Ann Arbor, Mich., 1946), Chap. VI, pp. 127–135.

[2] Wilson, P. E. and Spier, E. E., "Nonlinear pressure coupling in cylindrical shell analysis," AIAA J. **2**, 370–372 (1964).

[3] Grossman, W. B., "Investigation of maximum stresses in long, pressurized, cylindrical, shells," AIAA J. **1**, 1129–1132 (1963).

[4] Timoshenko, S., *Theory of Plates and Shells* (McGraw-Hill Book Co., Inc., New York, 1940), 1st ed.

[5] Pulos, J. G. and Salerno, V. L., "Axisymmetric elastic deformations and stresses in a ring-stiffened, perfectly circular cylindrical shell under external hydrostatic pressure," David Taylor Model Basin Rept. 1497 (September 1961).

[6] Short, R. D. and Bart, R., "Analysis for determining stresses in stiffened cylindrical shells near structural discontinuities," David Taylor Model Basin Rept. 1065 (June 1959).

[7] Kempner, J. and Salerno, V. L., "Analysis of the inelastic behavior of transversely reinforced cylindrical shells under hydrostatic pressure," Polytechnic Institute of Brooklyn Aerodynamics Lab. PIBAL Rept. 172 (August 1950).

[8] Pulos, J. G., "Structural analysis and design considerations for cylindrical pressure hulls," David Taylor Model Basin Rept. 1639 (April 1963).

LITVC System Response Evaluation by Pressure Integration Methods

A. W. Langill Jr.

Aerojet-General Corporation, Sacramento, Calif.

THE injection of fluids into the diverging portion of rocket nozzles to obtain side force for vehicle guidance has received considerable attention over the past few years. To characterize the complete liquid injection thrust vector control (LITVC) system response under conditions of dynamic excitation, an injection program consisting of a series of variable frequency flow-rate oscillations, superimposed upon a steady-state level (Fig. 1), is often implemented. The problem is to measure, with reasonable accuracy, the sinusoidal flow-rate excitation and resulting side-force response.

The typical thrust stand used to constrain the solid rocket motor during captive testing is a lightly damped, multiple-degree-of-freedom spring-mass system exhibiting relatively low natural frequency parameters. Because of the poor damping qualities, the undistorted direct side-force measurement system bandwidth is limited to 10 or 25% of the lowest resonant frequency (depending upon the particular definition

Presented as Preprint 64-505 at the AIAA 1st Annual Meeting, Washington, D. C., June 29–July 2, 1964; revision received November 10, 1964.

* Technical Specialist, Solid Rocket Operations Test Division. Member AIAA.

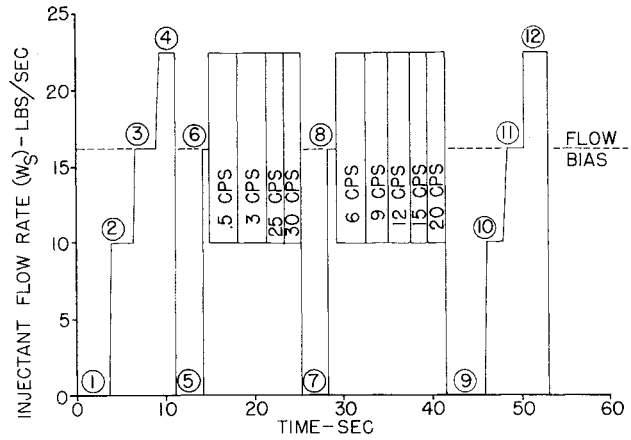

Fig. 1 Liquid injection program for dynamic response motor firing.

of "undistorted"). Since the maximum side-plane excitation frequency is often three or four times the lowest stand resonance, severe distortion in both amplitude and phase parameters occurs throughout the frequency range of interest. However, an indirect, instantaneous side-force measurement capability can be established by equating the side force to a corresponding internal nozzle-pressure integral. Total side force, due to liquid injection, is thus the sum of the pressure integral derived force level plus the momentum forces generated by the liquid.

Physical Test Environment

In the LITVC flow-rate program (Fig. 1), the initial and final portions consisted of a series of steady-state flow-rate null and plateau regions, whereas the intermediate portion was comprised of excitation frequencies extending from 0.5 to 30 cps. The time intervals allocated to data points 1–13 allowed an accurate direct side-force measurement; these program nulls provided a method for "calibrating" the corresponding pressure contour integral.

A multicomponent thrust stand was employed to constrain the solid rocket motor. In addition to the axial force cell, fore and aft side-plane force transducers were provided to measure the motor-generated side force. The use of modular flexure isolation and optimally sized force transducers resulted in relatively low thrust stand undamped natural frequency and damping characteristics.

A 52-nozzle-pressure-tap configuration (Fig. 2) provided the means for determining the internal nozzle-pressure distribution throughout the firing duration. All pressure taps were located in a single nozzle quadrant, thus insuring substantial coverage of a relative large geometric area. The

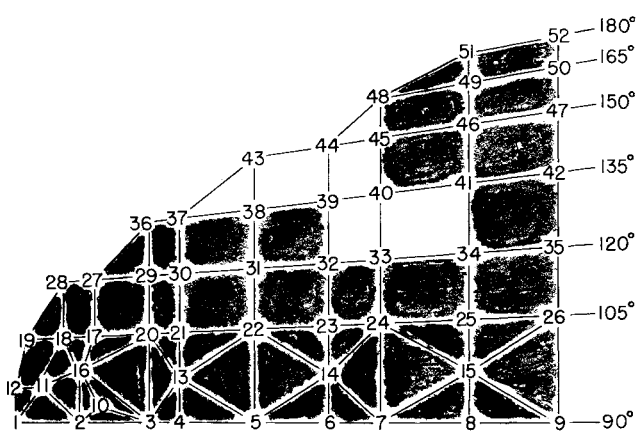

Fig. 2 Nozzle-pressure-tap locations.

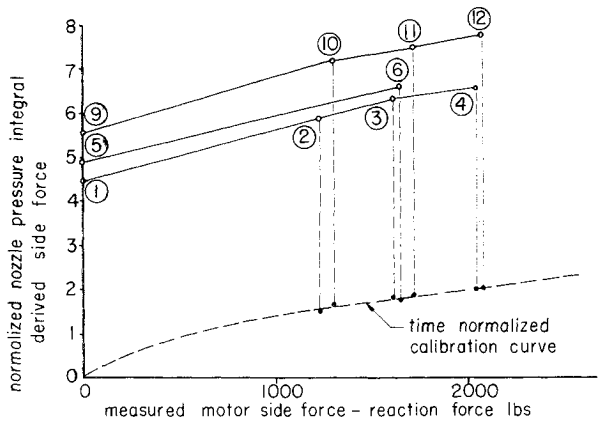

Fig. 3 Nozzle-pressure-integral calibration curve (normalized to a constant value of chamber pressure).

nozzle contour diagram of Fig. 2 was generated by means of an IBM-1401 computer program and reflects a projection of the nozzle geometry into the side plane.

Instrumentation and Data Acquisition Systems

A Ramapo Mark V high-frequency-response bending beam flowmeter was employed in the measurement of injectant flow. Dynamic calibration data, involving the actual LITVC flow system, were completed prior to the motor firing. Based upon Ramapo flowmeter tests, the typical Mark V amplitude ratio curve has a flat response from d.c. through 35% of the predominant undamped natural frequency. The damped natural frequency of the unit employed in this work was approximately 200 cps; thus the transducer could be considered flat to at least 70 cps, a value greater than twice the highest program frequency of Fig. 1. Since the Ramapo flowmeter exhibited a nonlinear input-output relationship (square-law), a six-line-segment linear interpolation program was mechanized to allow automatic digital data reduction.

Data Sensor model PB413B differential pressure transducers were close-coupled to each of the nozzle-pressure-tap points and rigidly mounted to the rocket nozzle. The transducer dynamic response was evaluated by a series of Wiancko shock generator calibrations. Calibration data analysis indicated a decay time (90 to 10% of the initial pressurization level) of 0.3 msec; the transducer was characterized as a second-order system with a damping ratio of approximately 0.7. The system bandwidth (−3 db point) was in excess of 60 cps. Transducer acceleration sensitivity was determined by shaking the unit along its most sensitive axis with a 40 g peak-to-peak acceleration and monitoring the electrical output. The response indicated a second-order system with an undamped natural frequency of 460 cps and a damping ratio of 0.18. The effect of temperature upon the data sensor output voltage was obtained by subjecting a transducer to the true thermal environment; in a motor firing preceding the subject test, a model PB413B unit was physically sealed prior to installation on the rocket nozzle. A gradual increase in the transducer output level (zero shift) was noted throughout the firing duration because of transducer temperature sensitivity.

Considerable attention was directed toward the selection of a suitable data acquisition system. Data are normally acquired, at Aerojet, in digital form by sampling the continuous output voltage from each transducer with an analog-to-digital converter (Beckman 210 system). However, the high sampling rate requirement and the large number of channels desired precluded the use of this acquisition technique; all data were thus recorded on oscillograph and later digitized by manual sampling. To minimize environmental effects and to attenuate all noise disturbances, a low-frequency-response galvanometer (CEC-7-315) was chosen for each channel. Since all data were processed through an identical data acquisition system, no relative phase shift or amplitude attenuation occurred in any measured parameters.

Baldwin-Lima-Hamilton U3XXA force cells were installed to monitor both fore and aft side-plane force levels. Although the total motor-generated side force could not be adequately computed (by a direct summation) during oscillatory flow sections of the program, the steady-state program regions allowed the nozzle-pressure integral to be calibrated against an accurately measured quasi-static force level.

The dynamic response motor was successfully test fired over the full intended duration. A postfire data analysis was conducted to determine the validity of all nozzle pressure measurements. Based upon this investigation, the shaded nozzle area of Fig. 2 was selected for integration. A semi-automatic data reduction of all pressure and flow-rate information was next accomplished; the OSCAR technique was employed to convert all flow-rate, force, and nozzle-pressure data to a punched-card format. Averaged single-point readings were taken in all steady-state null and plateau regions, and portions of each oscillatory program section were reduced with an effective 1000-cps sampling rate.

Digital Computer Processing

The underlying expression, relating the nozzle-pressure contour integral to total side force, is

$$K\int \Delta P_{ne} dA = F_{\text{side}} - F_{\text{reac}} \qquad (1)$$

where ΔP_{ne} is instantaneous pressure across the nozzle (internal nozzle pressure diminished by the ambient pressure), F_{side} is the total motor-generated side force, and F_{reac} is the fluid momentum component. Only a portion of the rocket nozzle was instrumented with nozzle-pressure transducers. Hence, it was necessary to define a pressure integral "scale factor," i.e., the quantity K of Eq. (1). The scale-factor calculation was mechanized for IBM-1401 computer simulation; data (punched) cards for all steady-state portions of the injection program were employed as input into the program. The computer then calculated 1) the nozzle-pressure force integral, based upon nozzle areas and differential pressure readings; 2) the reaction force; and 3) the algebraic summation of the two side-plane force cell levels, i.e., the total motor-generated side force. The force integral values were next normalized to an operating chamber pressure of 500 psi. Computer print-out consisted of the normalized force integral and the total measured side force diminished by the reaction force.

Calibration curves constructed from the results of this program are illustrated in Fig. 3. Note that the calibration exhibits a time-varying zero shift attributed to the nozzle-pressure transducer temperature sensitivity. Each data point number corresponds to the similar sequence of Fig. 1.

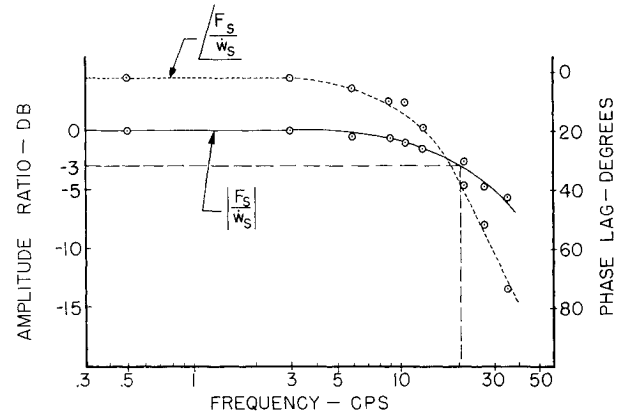

Fig. 4 LITVC system internal aerodynamic frequency response.

The data points were next normalized for time variance by linear interpolation, and the calibration curve resulting from this data processing procedure is plotted as the dashed overlay curve of Fig. 3.

A second digital computer program was written to reconstruct side force during the oscillatory portions of the flow program. The normalized calibration curve of Fig. 3 was programed for digital simulation; at any time point, then, the total pressure integral and reaction force variables were first defined. After normalizing the force integral to a consistent 500-psi chamber pressure and time adjusting, the computer determined the value of total side force diminished by the reaction force from Fig. 3. The final side force was obtained by summing the reaction force component to the previous calculation results. This routine was repeated at each of the remaining time points.

Although the final internal aerodynamic frequency response shows a rapid amplitude attenuation at the higher frequencies, the LITVC system internal aerodynamic bandwidth is flat to 20 cps (see Fig. 4). Both phase and amplitude ratio parameters are characteristic of a first-order system with a 20-cps break frequency.

Conclusions

Based upon results of this study, the following conclusions can be stated: 1) the pressure integral method of obtaining dynamic side-force response data appears attractive from an experimental viewpoint; manual data reduction could be greatly minimized, however, by recording all data on magnetic tape, with playback; 2) the Data Sensor differential pressure transducer is suited for the present application, although acceleration sensitivity could present problems for nozzle resonant frequencies in the neighborhood of 460 cps; 3) difficulties associated with pressure transducer temperature sensitivity and the resulting zero shift phenomena can be obviated by providing sufficient calibration null and plateau regions during the motor firing duration; and 4) the application of a consistent low-pass data acquisition system in all channels of information is desirable from a noise-rejection standpoint.

Conical Rocket Nozzle Performance under Flow-Separated Conditions

SHERWIN KALT* AND DAVID L. BADAL†
Lockheed Missiles and Space Company, Sunnyvale, Calif.

Nomenclature

A = cross-sectional area of the nozzle at a particular location, in.^{2}
c_f = nozzle thrust coefficient, with pressure on outside of motor assumed to be zero
F = thrust, lb
M = Mach number (in freestream)
M^* = characteristic M in boundary layer
p = static pressure at nozzle wall, psia
U = component of fluid velocity at edge of boundary layer parallel to wall, fps
u = component of fluid velocity in boundary layer parallel to wall, fps
u^* = characteristic velocity in boundary layer $\equiv 0.6\ U$
δ = boundary-layer thickness, in.
ϵ = nozzle-expansion ratio to a particular location
γ = specific-heat ratio of fluid
α = nozzle half-angle, deg

Subscripts

a = ambient conditions
c = combustion chamber, or reservoir conditions
e = nozzle-exit plane conditions; p_e applies in absence of separation
i = conditions at initiation of shock-turbulent boundary-layer interaction
s = conditions at separation of flow
t = conditions at nozzle throat
sl = sea-level conditions
0.95 = conditions at position in nozzle where static pressure equals 0.95 ambient pressure

Received June 12, 1964; revision received November 17, 1964. The work reported here was done under U. S. Navy Contract NOW-63-0050c.

* Research Specialist, Propulsion.
† Flight Test Analysis Engineer.

Introduction

ROCKET motors designed for high-altitude use are frequently tested under off-design conditions, for example at sea level, where it is expected that the flow in the rocket nozzle will show separation for a substantial portion of the test. For a design-performance extrapolation, using the ballistic data obtained from these tests, a means must be available to describe mathematically the flow separation conditions encountered. This note defines the necessary correlations for conical nozzles based on published data and on data from a series of flow separation tests using small 5KS-4500 motors (supplied by Aerojet-General Corporation) loaded with approximately 100 lb of aluminized solid propellant. The results, presented as part of Fig. 1, are consistent with the results of others[8–15] for such fluids as liquid propellant, air, and nitrogen in nozzles with various half-angles and expansion ratios at various ambient pressures.

Arens and Spiegler[1] present an equation adapted from one first suggested by Gadd[3] which shows the pressure ratio that would result if the fluid at velocity u_i^* in a constant stagnation temperature boundary layer were brought to rest isentropically, where $u_i^* = 0.6\ U_i$. The corresponding pressure rise $p_i - p_a$ is assumed to be equal to the resultant static pressure rise at the wall. On a semiempirical basis, Gadd chose a ratio $u_i^*/U_i = 0.6$ to calculate $p_i - p_s$, the pressure rise, from the point of the initiation of the shock-turbulent boundary layer to the separation point. In the case of a nozzle, the stagnation velocity will be most closely approached at ambient pressure, not at separation pressure, and therefore the derivation can be used to calculate $p_i - p_a$ for a nozzle. Arens and Spiegler[1] extend this concept to the supersonic case where the fluid in the boundary layer initially at velocity u_i^* is subjected to normal shock before being brought to rest isentropically. Equation (5) of Ref. 1 is plotted in Fig. 1, and good correlation to the experimental data is shown.

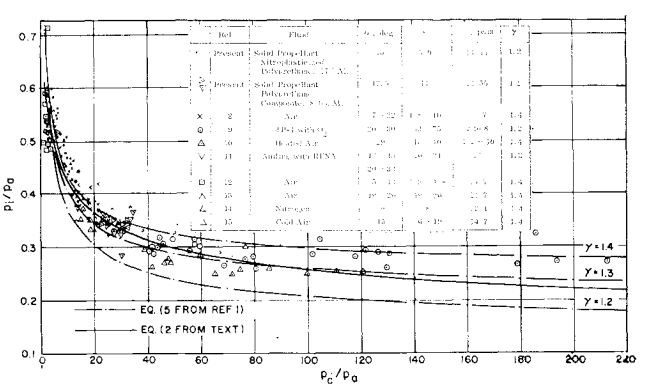

Fig. 1 Separation pressure ratio vs nozzle pressure ratio.